Research Square

Preprints are preliminary reports that have not undergone peer review.
They should not be considered conclusive, used to inform clinical practice,
or referenced by the media as validated information.

Easily separated and sustainable cellulose-based adsorbent using a facile two-steps modification for highly efficient methylene blue removal

Keming Zhou
East China University of Science and Technology
Lianpeng Yan
East China University of Science and Technology
Rui Zhang
r.zhang@ecust.edu.cn

East China University of Science and Technology
Xuedong Zhu
East China University of Science and Technology

Research Article

Keywords: Cellulose-based, Juncus effusus, Magnetic adsorbent, Dye adsorption

Posted Date: November 2nd, 2022

DOI: https://doi.org/10.21203/rs.3.rs-2215353/v1

License: This work is licensed under a Creative Commons Attribution 4.0 International License.
Read Full License

Additional Declarations: No competing interests reported.

Version of Record: A version of this preprint was published at Biomass Conversion and Biorefinery on February 23rd, 2023. See the published version at https://doi.org/10.1007/s13399-023-03885-8.

Abstract

Eco-friendly cellulose-based magnetic adsorbents have attracted great attention in the field of dye adsorption recently. Herein, we utilized the pith of biomass Juncus effusus (JE) to synthesize a novel type of magnetic adsorbents for the treatment of wastewater containing methylene blue (MB). After esterification and magnetization two-steps modification, the obtained magnetic citric acid-modified JE pith powders (M-CA/JEPP) showed outstanding adsorption properties. For 50 mg/L MB dye solution, the adsorption efficiency could reach 98.34% within 10 minutes under basic condition and the maximum adsorption capacity was 293.132 mg/g at 303 K. The adsorption efficiency could also keep a high level in five cycles. Moreover, magnetization overcomes the disadvantages of JE powders density being small which is very difficult to collect, and a 24.8 emu/g saturation magnetization was achieved. In the other words, this magnetic adsorbent has excellent reusability and it is easily to be separated from water, which provides new insights for development of cellulose-based adsorbents to remove dye in aqueous systems.

Introduction

Water shortage and pollution have threatened people's daily life all over the world. Therefore, improving the removal efficiency of water contaminants to make full use of water resources is of great practical significance to realize sustainable development [1, 2]. Organic dyes are widely used for dyeing in textile, papermaking, plastics, leather, food, cosmetics and other fields, which is one of the most concerned pollutants in the water. During dyeing process, 10–15% of the dyestuffs are discharged directly into the wastewater [3]. These organic dyes which are toxic, degradable and have stable structure pour into the hydrosphere with wastewater, causing great harm to the environment and human [4, 5]. In particular, methylene blue (MB) is a characteristic cationic dye that has been extensively used in various industries due to its outstanding water solubility and color stability. However, it not only endangers aquatic organisms, but also bring people health problems such as dermatitis, jaundice, nausea, vomiting, and allergies [6].

A variety of physical, chemical, and biological technology have been taken to treat dye wastewater [7], such as flocculation [8], oxidation [9], adsorption [10], ion exchange [11], membrane filtration [12], electrochemistry [13], biodegradation and phytoremediation [14], etc. Among these technologies, adsorption has attracted more attention because it is efficient, simple and relatively low cost [15]. Traditional adsorbents include activated carbon [16, 17], zeolite [18, 19], carbon nanotubes [20, 21], etc., most of them are limited in application due to their high operating costs and hard regeneration [22, 23]. So renewable, low-cost and non-toxic adsorbents are becoming increasingly popular and have broad prospects in the field of dye wastewater treatment [24, 25].

Some parts of many plants are inexpensive dye adsorbents inherently [26–28], but they always have low adsorption capacity. Recently, biochar derived from plants has been extensively studied to achieve better adsorption performance [29]. However, most of the biochar cannot be prepared without high-

temperature pyrolysis and inert atmosphere at present, which means high energy consumption and special equipment requirements [30, 31]. Thus, finding a suitable plants and using modification seems to be a more energy-saving and simple method to improve dye adsorption capacity [32]. For example, high cellulosic content and large amount of easily available hydroxyl groups renders plant structure susceptible for esterification [33, 34], oxidation [35, 36], grafting [37], or other chemical modification. Although the adsorption capacity of these modified cellulosic adsorbents has been improved, the low density which makes the separation and reuse process become a growing challenge.

Juncus effusus (JE) is a kind of cheap and accessible cellulose-based biomass whose pith have a 3D network structure naturally [38]. Though JE pith powders are born with dye adsorption ability, it still faces the above problems of low density and poor adsorption capacity. In this paper, we proposed a facile two-steps modification to solve these questions. Firstly, we introduced plenty of carboxyl functional groups into JE pith powders by citric acid-modification which increase the adsorption behavior obviously. Then a convenient solution of magnetization modify was conducted to endow this adsorbent with easily separated ability. Finally, the citric acid-modified JE pith powders loaded with Fe_3O_4 nanoparticles (M-CA/JEPP) showed great adsorption performance for cationic dye MB due to the plentiful active adsorption sites and the enhancement of the roughness on its surface after the two-step modification. To our best of knowledge, there were barely similar reports about this two-steps chemical modification towards natural plants for MB dye adsorption. The effects of different factors, such as pH, contact time, initial dye concentration and temperature on the adsorption performance were systematically evaluated, and the parameters of adsorption isotherms, thermodynamics and kinetics were obtained by fitting with classical models. Furthermore, the adsorption mechanism was also proposed based on the experiment. In all, the M-CA/JEPP which synthesized by two-step modification is a novel high performance cellulose-based adsorbent with excellent reusability and separation ability from wastewater. It may open the window for development of sustainable adsorbents to remove dye in wastewater treatment.

Experimental Section

Materials

Dry Juncus effusus pith powders (JEPP) were purchase from the local Chinese herb shop. Sodium hydroxide (NaOH) and citric acid (CA) were obtained from Shanghai Ling Feng Chemical Reagent Co., Ltd. Ferric trichloride ($FeCl_3·6H_2O$), ferrous sulfate ($FeSO_4·7H_2O$) and hydrochloric acid (HCl) were purchased from Sinopharm Chemical Reagent Co., Ltd. Ammonia solution ($NH_3·H_2O$, 25–28 wt%) was purchase from Shanghai Macklin Biochemical Co., Ltd. Methylene Blue (MB) was purchased from J&K Scientific Ltd.

Synthesis methods

Preparation of CA-modified JEPP (CA/JEPP)

Prior to CA modification, dry JEPP were screened using a 100 mesh sieve. Then 9 g of JEPP were added to 180 mL of 0.1 M NaOH solution, this alkali treatment was stirred at 65 ℃ for 1 h. After cooling to room temperature, the pre-treated JEPP were rinsed with deionized water until the pH of the filtrate dropped to neutral. Water was drained and the washed JEPP were dried in an oven at 50 ℃ for 24 h.

The esterification modification by CA was as follows: Briefly, 1.1 g of as-prepared JEPP were added to 11 mL of 0.6 M CA at room temperature with stirring for 30 minutes. After draining the liquid, the wet powders were placed in an oven at 50 ℃ for 24 h. Then the temperature of the oven was raised to 120 ℃, and this temperature was kept for 90 minutes. The modified JEPP were washed several times using hot deionized water about 70°C to remove excess citric acid. The wet powders are placed in an oven at 50 ℃ for 24 h, the dry products named CA/JEPP were milled and stored in a desiccator.

Synthesis of CA-modified magnetic JEPP (M-CA/JEPP)

The magnetic adsorbent M-CA/JEPP-1 was synthesized by a facile co-precipitation method that did not require an inert atmosphere [39]. 1.081 g of $FeCl_3 \cdot 6H_2O$ (2.5 mmol) and 0.695 g of $FeSO_4 \cdot 7H_2O$ (4.0 mmol) were dissolved in 100 mL distilled water to obtain a brownish-yellow mixed solution. 0.926 g of the CA/JEPP were added to the iron ions solution and stirred for 20 minutes at room temperature. Afterward, 20 mL of ammonia solution (25–28 wt%) was slowly dropped into the mixture with ultrasonic oscillations. The reaction was placed in a water bath at 70 ℃ and stirred for 1 h. After cooling the mixture to room temperature, the magnetic products were separated by magnet and washed with ethanol-water mixture for several times. Finally, the M-CA/JEPP were obtained after vacuum drying at 60°C for 6 h. The different doses of $FeSO_4 \cdot 7H_2O$ and $FeCl_3 \cdot 6H_2O$ were used to obtain M-CA/JEPP-2 and M-CA/JEPP-3. More information was shown in **Table S1** and **Fig. S1.** M-CA/JEPP-1 was selected as the most effective adsorbent and re-named as M-CA/JEPP which was further used in the following experiments.

Characterization

The fourier transforms infrared spectroscopy (FTIR) analysis of the samples were performed on a FTIR spectrometer (Nicolet IS50, Thermo Fisher Scientific, USA) at room temperature in the range of 4000 – 400 cm^{-1}. X-ray diffraction measurements were tested on an X-ray diffractometer (XRD, D8 Advance Bruker, Germany) using Cu Kα radiation in the range of 2θ = 5–80° with a scanning rate of 10 °/min. The X-ray photoelectron spectroscopy (XPS) spectra were carried out by a Thermo Scientific K-Alpha with a monochromatic source of X-rays (Al Kα, hv = 1486.6 eV). The morphologies of JEPP and M-CA/JEPP were observed on a Field emission scanning electron microscopy (FE-SEM, Sigma300, ZEISS, Germany) and energy dispersive spectroscopy (EDS) coupled with SEM was used. The particle size and distribution of Fe_3O_4 loaded on the adsorbent were analyzed by transmission electron microscopy (TEM, TF20, Thermo Fisher Scientific, USA). Magnetic properties were obtained using a vibrating sample magnetometer LakeShore7404 (VSM, LakeShore, USA) at room temperature. The specific surface area of the sample was. characterized by Brunauer-Emmett-Teller (BET) tests using a specific surface area and porosity analyzer (ASAP2460, Micromeritics, USA).

Batch adsorption experiments

Dry magnetic adsorbents were used for adsorption experiments. Typically, 10 mg of M-CA/JEPP were added into 20 mL of MB dye solution of known concentration at certain temperature, followed by shaking in a water bath shaker at 200 rpm. After adsorption, the adsorbents were separated from mixture by a magnet. The residual concentration of MB was determined by a UV visible spectrophotometer (UV-2550, Shimadzu, Japan) at 664 nm. Each experiment was carried out in triplicate. The amount of dye adsorbed at time t (q_t) (mg/g) or at equilibrium (q_e) (mg/g) and the adsorption efficiency (%) were calculated using Eq. 1–3:

$$q_t = \frac{(C_0 - C_t)\,V}{m}$$

1

$$q_e = \frac{(C_0 - C_e)\,V}{m}$$

2

$$\mathrm{adsorptionefficiency} = \frac{(C_0 - C_e)}{C_0} \times 100\%$$

3

where C_0, C_e and C_t (mg/L) are the initial, at time t and equilibrium concentration of dye solution, respectively, V (L) is the volume of solution, and m (g) is the mass of the adsorbent.

For the initial pH impact study, 10 mg of M-CA/JEPP were added into a flask containing 20 ml of MB solution (100 mg/L) at different initial pH, ranging from pH 4 to 11. The initial pH was adjusted with 0.1 M HCl or 0.1 M NaOH. In order to evaluate the effect of initial dye concentration on adsorption, various dye solution containing 100–500 mg/L of MB were prepared for adsorption. The concentration of MB during adsorption process were measured at predetermined time intervals to study the influence of contact time. Adsorption kinetics, isotherms and thermodynamics were also conducted to investigate the adsorption performance and mechanisms.

Reusability experiments

After adsorption (initial dye concentration was 50 mg/L), 10 mg of adsorbents were separated by a magnet and regenerated with 10 mL of 0.1 M HCl in a rotary shaker at 200 rpm for 20 minutes at 30°C. Then the adsorbent was rinsed several times using deionized water and was placed in a vacuum oven at 60°C for 6 h to obtain the regenerated adsorbent. The regenerated adsorbent was added to 50 mg/L MB solution again as the next adsorption cycle. And the reusability of M-CA/JEPP was performed as described above for five cycles.

Results And Discussion

Preparation of M-CA/JEPP

The synthesis of magnetic bio-adsorbent M-CA/JEPP derived from Juncus effusus was illustrated in Scheme 1. During pretreatment, dry JEPP were washed by alkali to remove contaminants and reduce hemicelluloses and lignin contents [40]. Then citric acid was dehydrated to obtain anhydride under 120 ℃ and combined with the hydroxyl groups in the cellulose to form an ester linkage to endowed the biomass with carboxyl groups [41, 42]. Finally, the magnetic particles were loaded on cellulose by chemical co-precipitation to fabrication the adsorbent.

Chemical structure and morphology characterization of M-CA/JEPP

The functional groups of JEPP, CA/JEPP and M-CA/JEPP and their positions were determined by FTIR. As shown in Fig. 1a, a broad peak between 3000–3700 cm^{-1} was linked to -OH stretching vibrations involved in the hydrogen bond interaction [43]. The absorption peaks observed at 2922 cm^{-1} and 2848 cm^{-1} corresponded to C-H stretching vibrations from CH and CH_2 in cellulose, hemicellulose and lignin. Similarly, multiple peaks in the regions between 1000–1800 cm^{-1} were related to the functional groups in cellulose, hemicellulose and lignin of the plant. Among them, the peak centered at 1736 cm^{-1} was attributable to the C = O stretching of hemicelluloses, the peak located at 1513 cm^{-1} was associated with C = C groups from lignin and the peak around 1250 cm^{-1} came from C–O stretching in lignin and hemicelluloses [40, 44, 45]. The peaks of CA/JEPP near 1250 cm^{-1} and 1513 cm^{-1} were dramatically reduced, indicating a decrease in lignin and hemicellulose, which may be due to the alkali treatment, while a significant enhancement of the peak at 1736 cm^{-1} could prove that citric acid have reacted with cellulose successfully. After magnetizing, the visible peak of M-CA/JEPP around 580 cm^{-1} belonged to Fe-O bonds in Fe_3O_4, and the peak appeared at 1400 cm^{-1} indicated the presence of COO^-. The peak of C = O vibration from citric acid moved from 1736 cm^{-1} to 1613 cm^{-1} because of the influence of covalent bonds on the surface of Fe_3O_4 [46], implying the interaction existed in Fe_3O_4 and citric acid.

The X-ray diffraction patterns were conducted to identify the crystal structure of JEPP and M-CA/JEPP (Fig. 1b). Weak and broad peaks of the origin JEPP around 16.7° and 22.6° represented the amorphous region and crystalline area of cellulose [40]. The XRD pattern of M-CA/JEPP exhibited the typical diffraction peaks of trans spinel structure which was consistent with Fe_3O_4. The characteristic peaks at 30.2°, 35.5°, 43.2°, 53.7°, 57.1° and 62.7° were attributed to (220), (311), (400), (422), (511), (440) crystal planes, respectively [47].

To analyze the chemical composition and electronic states of various elements, XPS analysis was also performed and the results were compiled in Fig. 1c-f. The presence of carbon, oxygen, and iron peaks

was confirmed by the XPS wide-scan survey of M-CA/JEPP (Fig. 1c). In the high-resolution XPS spectrum for C1s (Fig. 1d), there were three peaks located at 284.8 eV, 286.5 eV, and 288.1 eV attributing to C-C, C-O, and C = O/O = C-O [48], respectively. The high-resolution XPS spectrum for O1s (Fig. 1e) could be deconvoluted into four individual peaks around 530.0 eV, 531.3 eV, 532.8 eV and 533.1 eV which was corresponded to Fe-O, C = O/O = C-O, O-H, and C-O [48, 49], respectively. The Fe2p spectrum (Fig. 1f) showed two main peaks at 710.3 and 724.9 eV, which could be assigned as $Fe2p_{3/2}$ and $Fe2p_{1/2}$ from Fe_3O_4 [50] The deconvoluted peaks of Fe2p spectrum were linked to octahedral Fe^{3+} species, tetrahedral Fe^{3+} species, satellite peak of Fe^{3+} and Fe^{2+} ions, and octahedral Fe^{2+} species [51, 52]. Combined the results of FTIR, XRD and XPS, it could indicate that magnetic Fe_3O_4 was synthesized and incorporated into the CA-modified JEPP successfully.

The microstructure and surface morphology of initial JEPP and M-CA/JEPP were characterized by SEM. As shown in Fig. 2a, JEPP presented the shape of framing scaffold structure and smooth surface. Micro pores could be observed on the framing scaffold structure which were several microns in size. After modification and magnetizing, the surface of obtained M-CA/JEPP became extremely rough with the large pores disappeared, but some cracks and pits which might be conducive to adsorption were formed (Fig. 2b, d, e). The EDS spectra of M-CA/JEPP (Fig. 2c) only exhibited the peaks of C, O, and Fe, which were three major constituents of CA-modified fibers and magnetite, confirming there hasn't impurities introduced during the synthesis process. Additionally, Fig. 2e showed there were plenty of magnetic nanoparticles covering on the surface of modified JEPP and the specific surface area was 34.15 m^2/g (**Fig. S2**). Moreover, the EDS mapping were performed (Fig. 2f). The resulting patterns showed that C, O, Fe elements were uniformly distributed throughout the adsorbent powders, which was strong evidence for the combination of Fe_3O_4 and CA/JEPP.

The size and distribution of magnetic nanoparticles on adsorbents were shown in TEM images (**Fig. S3a, b**). The Fe_3O_4 nanoparticles were evenly distributed on the surface of the powders, whose average size was 6.60 nm (**Fig. S3d**). There was no serious aggregation between those nanoparticles. The ultrasonic assistance and citric acid modification in the fabrication process could reduce the possibility of aggregation and was beneficial for better dispersion [53]. As presented in high-resolution transmission electron microscopy (HRTEM) image (**Fig. S3c**), the lattice fringes of the samples displayed interplanar spacings of 0.254 nm and 0.302 nm in the nanoparticles, which matched well respectively with the (311) and the (220) characteristic lattice planes of Fe_3O_4 [54].

Adsorption properties of the adsorbent

Effects of initial pH on MB adsorption

The initial pH value of the dye solution is a significant influencing factor for adsorption performance. Alkaline conditions were conducive to the adsorption of MB dyes by M-CA/JEPP. It could be seen from Fig. 3a that the adsorption efficiency of MB was gradually enhanced with pH increasing from 4 to 11. At pH 4, the adsorption efficiency of MB was 77.61%, while the adsorption efficiency of MB increased to

98.62% at pH 11. Similarly, Fig. 3b implied that the adsorption capacity was increased from 155.22 mg/g to maximum value (197.25 mg/g) while the pH was adding up from 4 to 11. Therefore, pH = 11 was chosen to study the adsorption properties in other experiments.

The pH of the solution will affect the dissociation of functional groups on the surface of M-CA/JEPP, which has a corresponding effect on the adsorption behavior. Under the acidic condition with low pH, more free hydrogen ions (H^+) in the solution competed with the cationic MB molecules to occupy the active site of the adsorbents, which inhibited the adsorption of MB [55]. As the pH rose from 4 to 11, the numbers of OH^- ions in the solution increased, promoting the dissociation of H^+ ions which came from -OH and -COOH functional groups on the surface of M-CA/JEPP. The electronegativity of the adsorbent enhanced, and the adsorption efficiency and adsorption capacity became higher owing to the electrostatic attraction between cationic dye and adsorbents.

Effects of contact time on MB adsorption

The contact time between adsorbents and dyes always affects the final result of the adsorption. Figure 3c presented rapid adsorption of dye in the first 10 minutes, for MB dye solution with initial concentrations of 50 mg/L, 100 mg/L, 150 mg/L, the adsorption efficiency could reach 98.34%, 95.21%, 88.93%. Thereafter, the adsorption efficiency increased gradually, and the adsorption quickly reached equilibrium in around 60 minutes. With increasing of initial dye concentration, the adsorption capacity could reach up to a higher equilibrium value with time increasing (Fig. 3d). But the increased in contact time has promoted the aggregation of dye molecules [56], which made it almost impossible to diffuse deeper into the adsorbent structure and hindered the unlimited increasing of adsorption capacity.

Effects of initial dye concentration on MB adsorption

The effect of initial dye concentration in the range of 10 to 500 mg/L was investigated and the results were shown in Fig. 3e, f. As the initial dye concentration increased, the adsorption efficiency declined (Fig. 3e). While the adsorption efficiency for MB was found to be 98.62% for 100 mg/L of initial concentration, the value was 28.82% with the initial dye concentration was 500 mg/L. As shown in Fig. 3f, the adsorption capacity increased and finally tend to be stable with the initial dye concentration increasing. Since high initial dye concentration might provide the high driving force for the mass transfer [57], the adsorption capacity increased from 197.25 mg/g to 272.08 mg/g with the initial dye concentration changed from 100 mg/L to 150 mg/L. However, as the adsorbent dose was fixed, which meant the available active sites were limited, so the adsorption capacity would become similar if the initial dye concentration was higher than 150 mg/L.

Magnetic property and reusability of M-CA/JEPP

The M-CA/JEPP showed powerful magnetic property. The magnetization curve in Fig. 4a revealed the ferromagnetic behavior of M-CA/JEPP, its saturation magnetization was 24.8 emu/g, which was significantly stronger than 3.6 emu/g [58] and 5.0 emu/g [59] in other magnetic cellulose-based adsorbent works. Therefore, this new type of adsorbent showed powerful magnetic responsivity, and it

could be separated conveniently within ten seconds from the treated solution with the help of an external magnetic force (Fig. 4b). In other words, it can be used as a magnetic trigger to finish the separation and reuse process in wastewater treatment.

The cyclic adsorption experiment was performed to investigate the regeneration of the adsorbent (Fig. 4c). The adsorbent was regenerated by using 0.1 M HCl as desorption reagent after adsorption. The results showed that for 50 mg/L MB solution, the removal efficiency of the M-CA/JEPP towards MB could maintain a level above 98% after five cycles, which was hardly reduced, suggesting that the adsorbent had outstanding recyclability.

Proposed adsorption mechanism

In order to explore the adsorption mechanism of MB dye by M-CA/JEPP, the infrared spectrum tests were carried out (Fig. 4d). The absorption peaks of 1300–1430 cm^{-1} and 1600 cm^{-1} showed that MB was combined with the adsorbents. For M-CA/JEPP, the peak of COO^- groups migrated from 1400 cm^{-1} to 1393 cm^{-1}, while the absorption peak of –OH functional groups at 3420 cm^{-1} moved to 3411 cm^{-1}, indicating that the adsorption process involved electrostatic adsorption and hydrogen bonding [60, 61]. In addition, the role of pores and the π-π interaction between the benzene ring in MB molecule and the hexagonal skeleton of adsorbent [62] might also make important contributions to the adsorption.

Fitting results of the adsorption process

Adsorption kinetics

Four typical kinetic models including pseudo-first-order, pseudo-second-order, Elovich and intraparticle diffusion were conducted to calculate the rate constants and other parameters of the M-CA/JEPP for MB adsorption according to **Equation S1-S4**. The fitting results and parameters were shown in Fig. 5 and Table 1.

The correlation coefficient (R^2) was used to assess the degree of conformity between the experimental values and the theoretical values of the model. According to the fitting results of different concentrations of MB, the R^2 values calculated by the pseudo-first-order dynamic model were between 0.969–0.989. The R^2 values of the intraparticle diffusion model were between 0.577–0.977, and its fitted line were not zeroaxial, which indicated that intraparticle diffusion was not the rate-limiting step of the whole adsorption [34]. Elovich model was commonly used to deal with the chemical adsorption mechanism in nature, the R^2 values of Elovich model were in the range of 0.935–0.975 [63]. The R^2 values calculated by the pseudo-second-order dynamic model were above 0.996 and the obtained $q_{e,cal}$ values were also closest to the original experimental values. So pseudo-second-order model was more appropriate for defining this adsorption process, suggesting that the rate control step occurred during the entire adsorption process [64].

Table 1
Kinetic parameters for different initial concentrations of MB on M-CA/JEPP with various models

Kinetics models	Parameters	Initial concentration		
		50 mg/L	100 mg/L	150 mg/L
Pseudo-first-order	$q_{e,exp}$ (mg/g)	98.837	197.247	276.450
	$q_{e,cal}$ (mg/g)	97.678	192.348	267.360
	k_1 (min^{-1})	2.298	0.851	1.554
	R^2	0.989	0.986	0.969
Pseudo-second-order	$q_{e,exp}$ (mg/g)	98.837	197.247	276.450
	$q_{e,cal}$ (mg/g)	99.783	200.526	275.755
	k_2 [g/(mg min)]	0.050	0.006	0.010
	R^2	0.999	0.999	0.996
Elovich	α [mg/g min]	1.667E + 9	7.482E + 3	8.630E + 5
	β [g/mg]	0.237	0.049	0.053
	R^2	0.974	0.935	0.975
Intrapaticle diffusion	$k_{p,1}$ [mg/g $min^{-0.5}$]	29.089	95.758	86.421
	C_1 (mg/g)	51.373	12.256	107.896
	R^2	0.997	0.965	0.992
	$k_{p,2}$ [mg/g $min^{-0.5}$]	0.166	1.886	2.742
	C_2 (mg/g)	97.641	180.751	253.277
	R^2	0.938	0.577	0.649

Adsorption isotherm

Langmuir, Freundlich and Temkin adsorption isotherms were used to explain the relationship between the adsorbent and adsorbate according to **Equation S5-S7**. The fitting results and parameters were shown in Fig. 6 and Table 2.

The results of the MB adsorption experiment at different temperatures indicated that the increase in temperature will make the adsorption capacity lower. Langmuir isotherm model was the most suitable

model, whose R^2 values were above 0.982. The maximum adsorption capacity of M-CA/JEPP for MB at 303 K was 293.132 mg/g, which surpass many magetic adsorbents derived from plants (Table 3). The Langmuir isotherm is often used to describe monolayer adsorption on uniform surfaces, which is also based on the assumption that the adsorption energy at each point of the surface is the same and there is no interaction between the adsorbate molecules attached to the surface. The Freundlich isotherm which suppose the energy on the surface is uneven is often used to describe multilayer adsorption. Furthermore, The Temkin isotherms assume that the adsorption heat of all molecules in the layer will decrease linearly with coverage rate due to the adsorbent/adsorbent interaction, which is commonly used to explain the interaction between adsorbent molecules adsorbed on the surface [65, 66]. The optimal adaptation of the Langmuir isotherm substantiated that the MB adsorption by M-CA/JEPP was monolayer adsorption rather than multilayer adsorption. In addition, one essential characteristic of the Langmuir isotherm could be expressed by the separation factor R_L calculated from **Equation S8**. In the present study, R_L values were between 0–1, indicating that the adsorption process under experimental conditions is conducive to proceeding [67].

Table 2
Isotherm parameters for MB on M-CA/JEPP with various models at different temperature

Isotherm models	Parameters	Temperature		
		303 K	313 K	323 K
Langmuir	q_{max} (mg/g)	293.132	284.929	279.584
	k_l (L/mg)	1.124	1.159	1.076
	R^2	0.986	0.982	0.992
Freundlich	*1/n*	0.154	0.154	0.156
	k_f [(mg/g)/(mg/L)$^{1/n}$]	133.957	130.151	126.474
	R^2	0.782	0.787	0.813
Temkin	*B*	33.578	32.440	31.948
	A_T (L/g)	46.887	48.667	47.059
	R^2	0.876	0.876	0.903

Table 3
The M-CA/JEPP for MB compared with other reported magnetic adsorbents which derived from plants

Adsorbents	q_m (mg/g)	Reference
durian shell fiber-Fe_3O_4-MOF	53.31	[68]
magnetic rice husk ash	150.5	[69]
Fe_3O_4-loaded biochar from sorghum straw	166.67	[70]
Magnetic biochar nanocomposite from raw avocado peel	62.1	[71]
Seawater/K_2FeO_4-derived magnetic biochar from jackfruit peel	129.61	[72]
Magnetic biochar from agricultural waste	55.0	[73]
Fenton-modified biochar from rubber tree bark	258.14	[74]
Hydrochar magnetic adsorbents from Chinese medicine industry waste	60	[75]
Citric acid-modified Juncus effusus pith powders loaded with Fe_3O_4 nanoparticles	293.132	This work

Adsorption thermodynamic.

After the experimental data fitted by **Equation S9-S11**, the thermodynamic parameters (Gibbs free energy change (ΔG), enthalpy change (ΔH), entropy change (ΔS) of this adsorption process could be calculated, the fitting lines and the calculated results were displayed in **Fig. S4** and **Table S2**. Among the results, $\Delta G < 0$ proved that the adsorption was a spontaneous process. The Negative ΔH indicated that these processes were exothermic, which further confirmed that temperature increasing was not beneficial for the adsorption. $\Delta S > 0$ suggested that due to the increased randomness of the solution/solid interface, adsorbent/adsorbent composites are formed [76, 77]. Moreover, the absolute value of ΔH was between 0–84 kJ/mol, which meant this MB adsorption process could be mainly regarded as physical adsorption [78].

Conclusion

In summary, we have demonstrated a simple two-steps approach to obtain CA-modified magnetic cellulose-based adsorbent. Compared with original JEPP, M-CA/JEPP had a rougher surface and richer functional groups, so its adsorption performance was greatly improved. The adsorption process was proved to be a spontaneous and exothermic reaction, where the adsorption data fitted the Langmuir isotherm and the pseudo-second-order model well. It could quickly reach the adsorption equilibrium within tens of minutes, with a maximum adsorption capacity of 293.132 mg/g for MB at 303 K. The superior adsorption performance of M-CA/JEPP might be mainly attributed to electrostatic interaction and hydrogen bonding. Furthermore, this kind of adsorbents was easy to recycle with magnet and could

maintain preeminent reusability in five cycles, which was more in line with the requirements of environmental protection. These findings will expand our horizons for preparing cellulosic adsorbents from nature to deal with dye contamination in aqueous system.

Declarations

Ethics approval and consent to participate

Not applicable.

Consent for publication

Not applicable.

Availability of data and materials

The datasets used and analyzed during the current study available from the corresponding author on reasonable request.

Author contributions

All authors contributed to the study conception and design. Material preparation, data collection and analysis were performed by Keming Zhou. The first draft of the manuscript was written by Keming Zhou and all authors commented on previous versions of the manuscript. All authors read and approved the final manuscript.

Funding

This work was supported by the National Natural Science Foundation of China (21374029, 21776076), Open Research Fund of Shanghai Key Laboratory of Green Chemistry and Chemical Processes, East China Normal University and Fundamental Research Funds for the Central Universities (JKA01221712).

Competing interests

The authors have no relevant financial or non-financial interests to disclose.

Acknowledgments

This work is supported by the National Natural Science Foundation of China (21374029, 21776076) and the Open Research Fund of Shanghai Key Laboratory of Green Chemistry and Chemical Processes, East China Normal University. We also thank Fundamental Research Funds for the Central Universities (JKA01221712).

References

1. M. A. Shannon, P. W. Bohn, M. Elimelech, J. G. Georgiadis, B. J. Marinas, A. M. Mayes, Nature **452**, 301-310 (2008)
2. H. F. Chen, Y. Zhou, J. Y. Wang, J. Lu, Y. B. Zhou, J. Hazard. Mater. **389**, 121897 (2020)
3. M. B. Yeamin, M. M. Islam, A.-N. Chowdhury, M. R. Awual, J. Clean. Prod. **291**, 125920 (2021)
4. Z. C. Li, H. Hanafy, L. Zhang, L. Sellaoui, M. Schadeck Netto, M. L. S. Oliveira, M. K. Seliem, G. Luiz Dotto, A. Bonilla-Petriciolet, Q. Li, Chem. Eng. J. **388**, 124263 (2020)
5. L. W. Chen, Y. Y. Zhu, Y. M. Cui, R. Dai, Z. H. Shan, H. Chen, Chem. Eng. J. **405**, 124263 (2021)
6. A. H. Jawad, A. S. Abdulhameed, A. Reghioua, Z. M. Yaseen, Int. J. Biol. Macromol. **163**, 756-765 (2020)
7. G. Crini, E. Lichtfouse, Environ. Chem. Lett. **17**, 145-155 (2018)
8. A. K. Verma, R. R. Dash, P. Bhunia, J. Environ. Manage. **93**, 154-168 (2012)
9. K. Paździor, L. Bilińska, S. Ledakowicz, Chem. Eng. J. **376**, 120597 (2019)
10. X. L. Zhao, X. J. Wang, T. Lou, J. Hazard. Mater. **403**, 124054 (2021)
11. L. Cseri, F. Topuz, M. A. Abdulhamid, A. Alammar, P. M. Budd, G. Szekely, Adv. Mater. Technol. 2000955 (2021)
12. H. J. Zeng, Z. X. Yu, L. Y. Shao, X. H. Li, M. Zhu, Y. C. Liu, X. F. Feng, X. M. Zhu, Chem. Eng. J. **403**, 126281 (2021)
13. E. Brillas, C. A. Martínez-Huitle, Appl. Catal. B **166-167**, 603-643 (2015)
14. D. Bhatia, N. R. Sharma, J. Singh, R. S. Kanwar, Crit. Rev. Environ. Sci. Technol. **47**, 1836-1876 (2017)
15. M. A. Ahsan, V. Jabbari, M. A. Imam, E. Castro, H. Kim, M. L. Curry, D. J. Valles-Rosales, J. C. Noveron, Sci. Total Environ. **698**, 134214 (2020)
16. S. Wong, N. Ngadi, I. M. Inuwa, O. Hassan, J. Clean. Prod. **175**, 361-375 (2018)
17. H. F. Wang, Z. C. Li, S. Yahyaoui, H. Hanafy, M. K. Seliem, A. Bonilla-Petriciolet, G. Luiz Dotto, L. Sellaoui, Q. Li, Chem. Eng. J. **417**, 128116 (2021)
18. E. Alver, A. Ü. Metin, Chem. Eng. J. **200-202**, 59-67 (2012)
19. L. Aljerf, J. Environ. Manage. **225**, 120-132 (2018)
20. R. S. Aliabadi, N. O. Mahmoodi, J. Clean. Prod. **179**, 235-245 (2018)
21. W. X. Zhang, Q. Yang, Q. H. Luo, L. L. Shi, S. J. Meng, J. Clean. Prod. **242**, 118425 (2020)
22. A. Alsbaiee, B. J. Smith, L. L. Xiao, Y. H. Ling, D. E. Helbling, W. R. Dichtel, Nature **529**, 190-194 (2016)
23. N. Jiang, R. Shang, S. G. J. Heijman, L. C. Rietveld, Water Res. **144**, 145-161 (2018)
24. X. Y. Shao, J. Wang, Z. T. Liu, N. Hu, M. Liu, C. Duan, R. M. Zhang, C. L. Quan, Cellulose **28**, 9355-9367 (2021)
25. A. G. Varghese, S. A. Paul, M. S. Latha, Environ. Chem. Lett. **17**, 867-877 (2018)
26. M. Ş. Tanyildizi, Chem. Eng. J. **168**, 1234-1240 (2011)

27. X. L. Han, W. Wang, X. J. Ma, Chem. Eng. J. **171**, 1-8 (2011)
28. G. D. Değermenci, N. Değermenci, V. Ayvaoğlu, E. Durmaz, D. Çakır, E. Akan, J. Clean. Prod. **225**, 1220-1229 (2019)
29. B. Qiu, Q. Shao, J. Shi, C. Yang, H. Chu, Sep. Purif. Technol. **300**, 121925 (2022)
30. Y. Zhang, Y. Zheng, Y. Yang, J. Huang, A. R. Zimmerman, H. Chen, X. Hu, B. Gao, Bioresour. Technol. **337**, 125432 (2021)
31. F. Yu, F. Tian, H. Zou, Z. Ye, C. Peng, J. Huang, Y. Zheng, Y. Zhang, Y. Yang, X. Wei, B. Gao, J. Hazard. Mater. **415**, 125511 (2021)
32. Aruna, N. Bagotia, A. K. Sharma, S. Kumar, Chemosphere **268**, 129309 (2021)
33. S. X. Zhao, T. S. Zhou, Bioresour. Technol. **219**, 330-337 (2016)
34. D. Peng, S. P. Cheng, H. S. Li, X. T. Guo, Chemosphere **272**, 129963 (2021)
35. V. Halysh, O. Sevastyanova, S. Pikus, G. Dobele, B. Pasalskiy, V. M. Gun'ko, M. Kartel, Cellulose **27**, 8181-8197 (2020)
36. F. Tang, H. Yu, S. Yassin Hussain Abdalkarim, J. Sun, X. Fan, Y. Li, Y. Zhou, K. Chiu Tam, Chem. Eng. J. **395**, 125070 (2020)
37. P. Du, L. Xu, Z. Ke, J. Liu, T. Wang, S. Chen, M. Mei, J. Li, S. Zhu, J. Colloid Interface Sci. **616**, 12-22 (2022)
38. F. T. Liu, R. Lu, Q. M. Pan, ACS Sustain. Chem. Eng. **5**, 922-928 (2016)
39. G. R. Mahdavinia, S. Mousanezhad, H. Hosseinzadeh, F. Darvishi, M. Sabzi, Carbohydr. Polym. **147**, 379-391 (2016)
40. L. J. Xia, C. H. Zhang, A. M. Wang, Y. L. Wang, W. L. Xu, Cellulose **27**, 1909-1920 (2019)
41. M. S. Sajab, C. H. Chia, S. Zakaria, P. S. Khiew, Bioresour. Technol. **128**, 571-577 (2013)
42. B. Zhu, T. X. Fan, D. Zhang, J. Hazard. Mater. **153**, 300-308 (2008)
43. B. B. Lu, Y. Y. Bo, M. J. Yi, Z. Y. Wang, J. C. Zhang, Z. Y. Zhu, Y. L. Zhao, J. H. Zhang, Adv. Funct. Mater. **31**, 2102794 (2021)
44. M. Maache, A. Bezazi, S. Amroune, F. Scarpa, A. Dufresne, Carbohydr. Polym. **171**, 163-172 (2017)
45. S. N, R. I, R. T, Carbohydr. Polym. **195**, 566-575 (2018)
46. R. M. Ashour, R. El-sayed, A. F. Abdel-Magied, A. A. Abdel-khalek, M. M. Ali, K. Forsberg, A. Uheida, M. Muhammed, J. Dutta, Chem. Eng. J. **327**, 286-296 (2017)
47. V. K. Gupta, A. Nayak, Chem. Eng. J. **180**, 81-90 (2012)
48. D. W. Yuan, K. Cadien, Q. Liu, H. B. Zeng, J. Colloid Interface Sci. **552**, 659-670 (2019)
49. J. X. Li, S. Y. Chen, G. D. Sheng, J. Hu, X. L. Tan, X. K. Wang, Chem. Eng. J. **166**, 551-558 (2011)
50. S. Sitthichai, C. Pilapong, T. Thongtem, S. Thongtem, Appl. Surf. Sci. **356**, 972-977 (2015)
51. D. Wilson, M. A. Langell, Appl. Surf. Sci. **303**, 6-13 (2014)
52. J. W. Lu, F. L. Fu, L. Zhang, B. Tang, Chem. Eng. J. **346**, 590-599 (2018)

53. J. Liu, Z. K. Sun, Y. H. Deng, Y. Zou, C. Y. Li, X. H. Guo, L. Q. Xiong, Y. Gao, F. Y. Li, D. Y. Zhao, Angew. Chem. Int. Ed. Engl. **48**, 5875-5879 (2009)
54. A. A. Alqadami, M. Naushad, Z. A. Alothman, A. A. Ghfar, ACS Appl. Mater. Interfaces **9**, 36026-36037 (2017)
55. A. Kausar, S. U. Rehman, F. Khalid, A. Bonilla-Petriciolet, D. I. Mendoza-Castillo, H. N. Bhatti, S. M. Ibrahim, M. Iqbal, Int. J. Biol. Macromol. **209**, 576-585 (2022)
56. P. S. Kumar, S. Ramalingam, C. Senthamarai, M. Niranjanaa, P. Vijayalakshmi, S. Sivanesan, Desalination **261**, 52-60 (2010)
57. M. A. M. Salleh, D. K. Mahmoud, W. A. W. A. Karim, A. Idris, Desalination **280**, 1-13 (2011)
58. H. J. Gao, J. Du, Y. W. Liao, Cellulose **26**, 3285-3297 (2019)
59. S. J. Zhou, L. J. Xia, Z. Fu, C. H. Zhang, X. Y. Duan, S. Y. Zhang, Y. L. Wang, C. L. Ding, X. Liu, W. L. Xu, Carbohydr. Polym. **258**, 117690 (2021)
60. L. Liu, Z. Y. Gao, X. P. Su, X. Chen, L. Jiang, J. M. Yao, ACS Sustain. Chem. Eng. **3**, 432-442 (2015)
61. W. L. Meng, Z. Y. Ma, J. C. Shu, B. Li, P. X. Su, R. Wang, M. J. Chen, Z. H. Liu, K. H. Ai, Sep. Purif. Technol. **281**, 119496 (2022)
62. L. J. Leng, X. Z. Yuan, H. J. Huang, J. G. Shao, H. Wang, X. H. Chen, G. M. Zeng, Appl. Surf. Sci. **346**, 223-231 (2015)
63. T. Shahnaz, D. Bedadeep, S. Narayanasamy, Int. J. Biol. Macromol. **200**, 162-171 (2022)
64. H. Li, M. J. Li, F. Zheng, J. Wang, L. Chen, P. F. Hu, Q. Zhen, S. Bashir, J. L. Liu, J. Clean. Prod. **325**, 129322 (2021)
65. I. A. W. Tan, B. H. Hameed, A. L. Ahmad, Chem. Eng. J. **127**, 111-119 (2007)
66. D. D. Eslek Koyuncu, M. Okur, Sep. Purif. Technol. **257**, 117657 (2021)
67. E. Wibowo, M. Rokhmat, Sutisna, Khairurrijal, M. Abdullah, Desalination **409**, 146-156 (2017)
68. Z. Cai, Q. Liu, H. Li, J. Wang, G. Tai, F. Wang, J. Han, Y. Zhu, G. Wu, Int. J. Mol. Sci. **23**, 5900 (2022)
69. C. P. Lawagon, R. E. C. Amon, Environ. Eng. Res. **25**, 685-692 (2019)
70. J. Xie, R. Lin, Z. Liang, Z. Zhao, C. Yang, F. Cui, J. Environ. Chem. Eng. **9**, 105744 (2021)
71. E. Prabakaran, K. Pillay, H. Brink, Mater. Today Sustain. **18**, 100123 (2022)
72. Q. Wen, Y. Chen, X. Rao, R. Yang, Y. Zhao, J. Li, S. Xu, Z. Liang, Bioresour. Technol. **350**, 126860 (2022)
73. A. Zubrik, M. Matik, E. Mačingová, Z. Danková, D. Jáger, J. Briančin, L. Machala, J. Pechoušek, S. Hredzák, Chem. Eng. Process. **178**, 109016 (2022)
74. S. Xu, J. Li, Z. Yin, S. Liu, S. Bian, Y. Zhang, Bioresour. Technol. **315**, 123797 (2020)
75. X. Zhang, S. Liu, M. Wang, X. Ma, X. Sun, X. Liu, L. Wang, W. Wang, Fuel **326**, 125110 (2022)
76. D. Y. Yu, Y. J. Wang, M. H. Wu, L. Zhang, L. L. Wang, H. G. Ni, J. Clean. Prod. **232**, 774-783 (2019)
77. H. Chen, X. X. Wang, J. X. Li, X. K. Wang, J. Mater. Chem. A **3**, 6073-6081 (2015)

78. E. Errais, J. Duplay, F. Darragi, I. M'Rabet, A. Aubert, F. Huber, G. Morvan, Desalination **275**, 74-81 (2011)

Scheme 1

Scheme 1 is available in the Supplementary Files section.

Figures

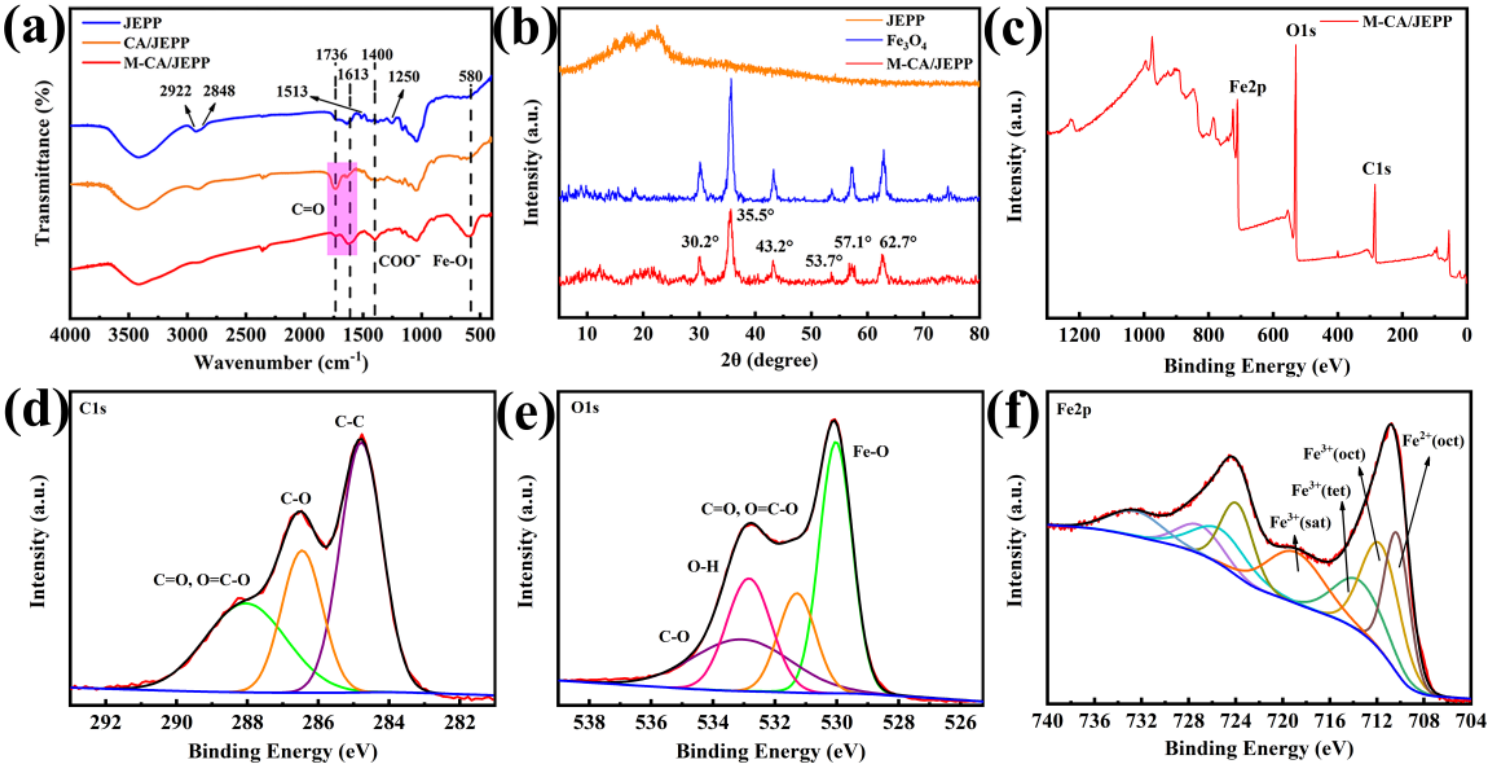


Figure 1

(a) FTIR spectra of JEPP, CA/JEPP and M-CA/JEPP. (b) XRD patterns of JEPP, Fe_3O_4 and M-CA/JEPP. (c) Wide-scan XPS spectra of M-CA/JEPP; High-resolution XPS spectra of (d) C1s, (e) O1s, (f) Fe2p for M-CA/JEPP

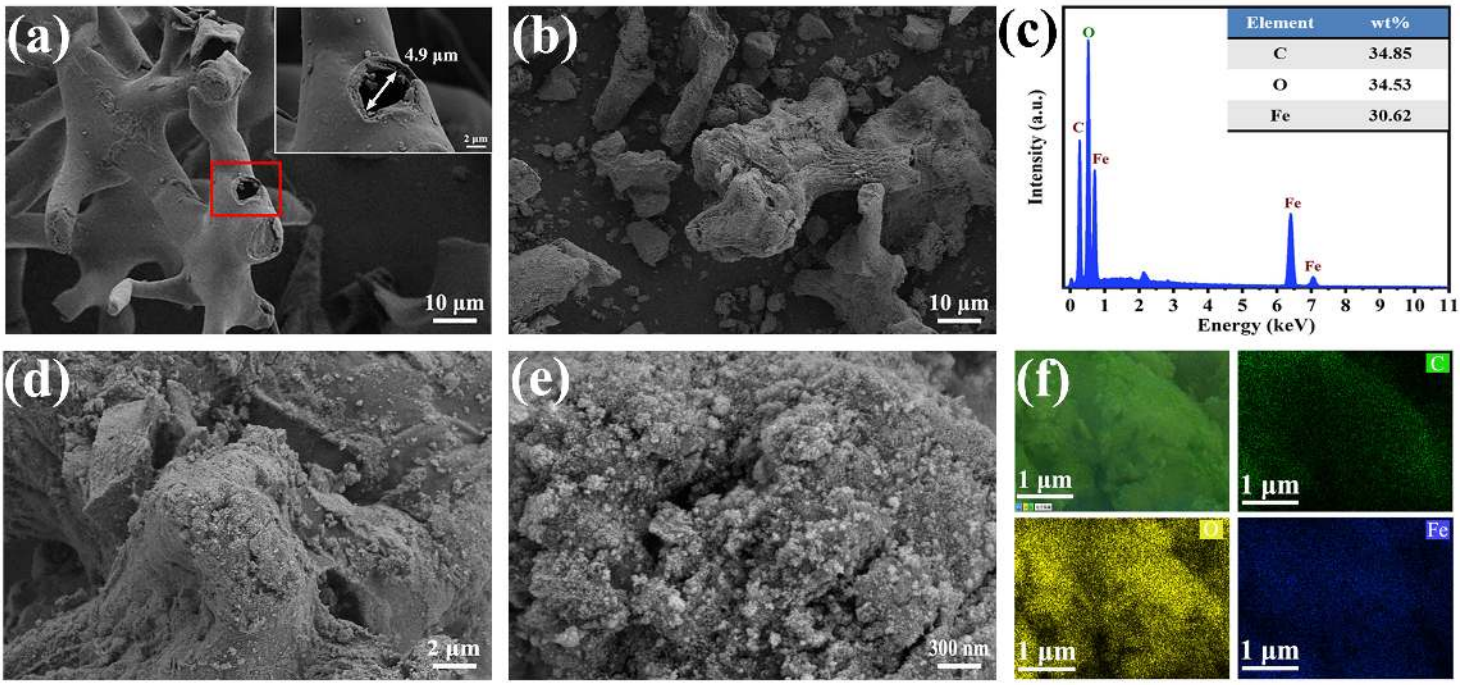


Figure 2

SEM images of (a) JEPP (b, d, e) M-CA/JEPP; (c) EDS analysis of M-CA/JEPP. (f) EDS mapping of M-CA/JEPP

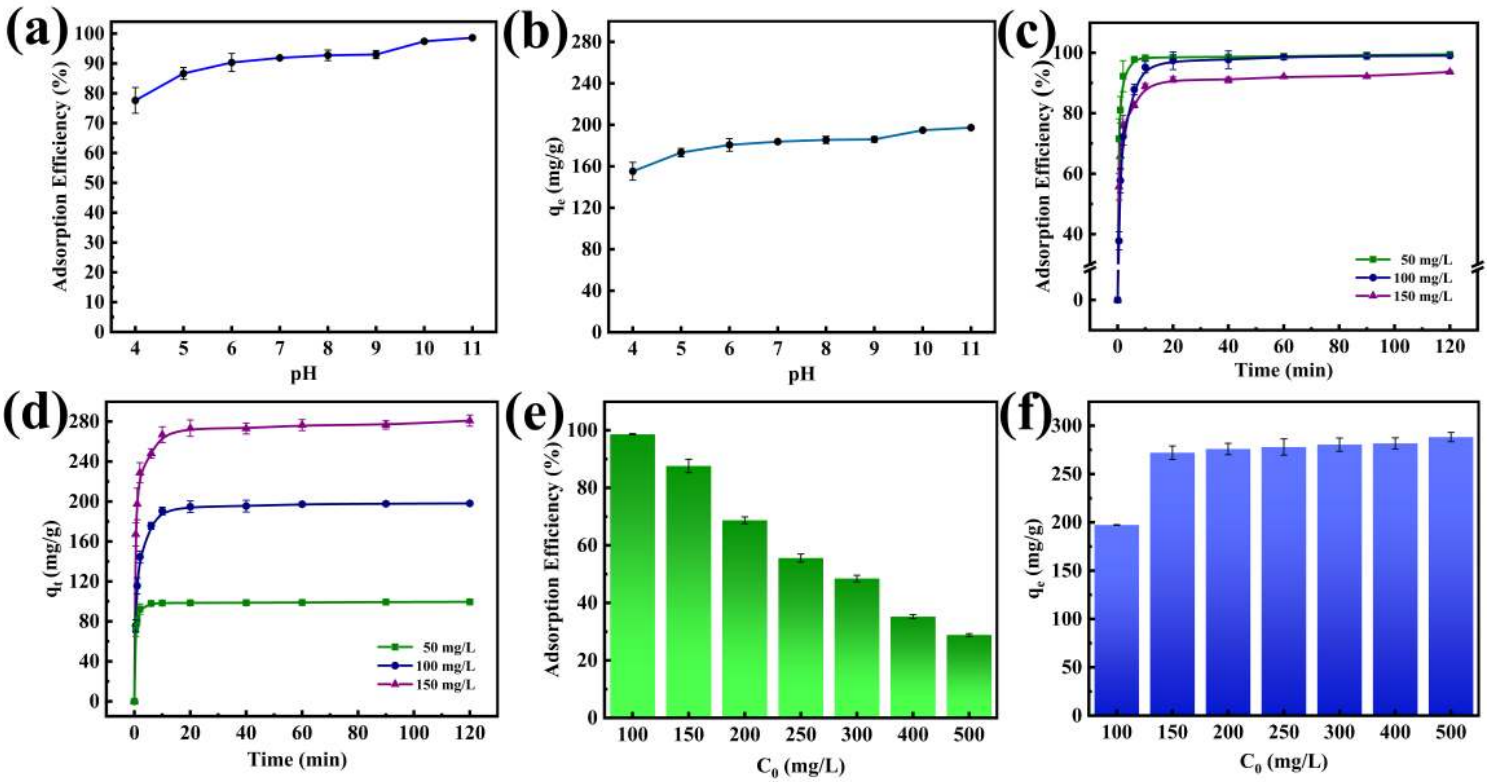


Figure 3

The adsorption efficiency (a) and the equilibrium adsorption capacity (b) of MB at different initial pH (4-11), initial dye concentration of 100 mg/L, 303 K and 10 mg of adsorbents. The adsorption efficiency (c) and the adsorption capacity (d) of MB in different time, initial pH=11, initial dye concentration of 50 mg/L, 100 mg/L and 150 mg/L, 303 K and 10 mg of adsorbents. The adsorption efficiency (e) and the equilibrium adsorption capacity (f) of MB towards different initial dye concentration in 60 minutes, initial pH=11, 303 K and 10 mg of adsorbents

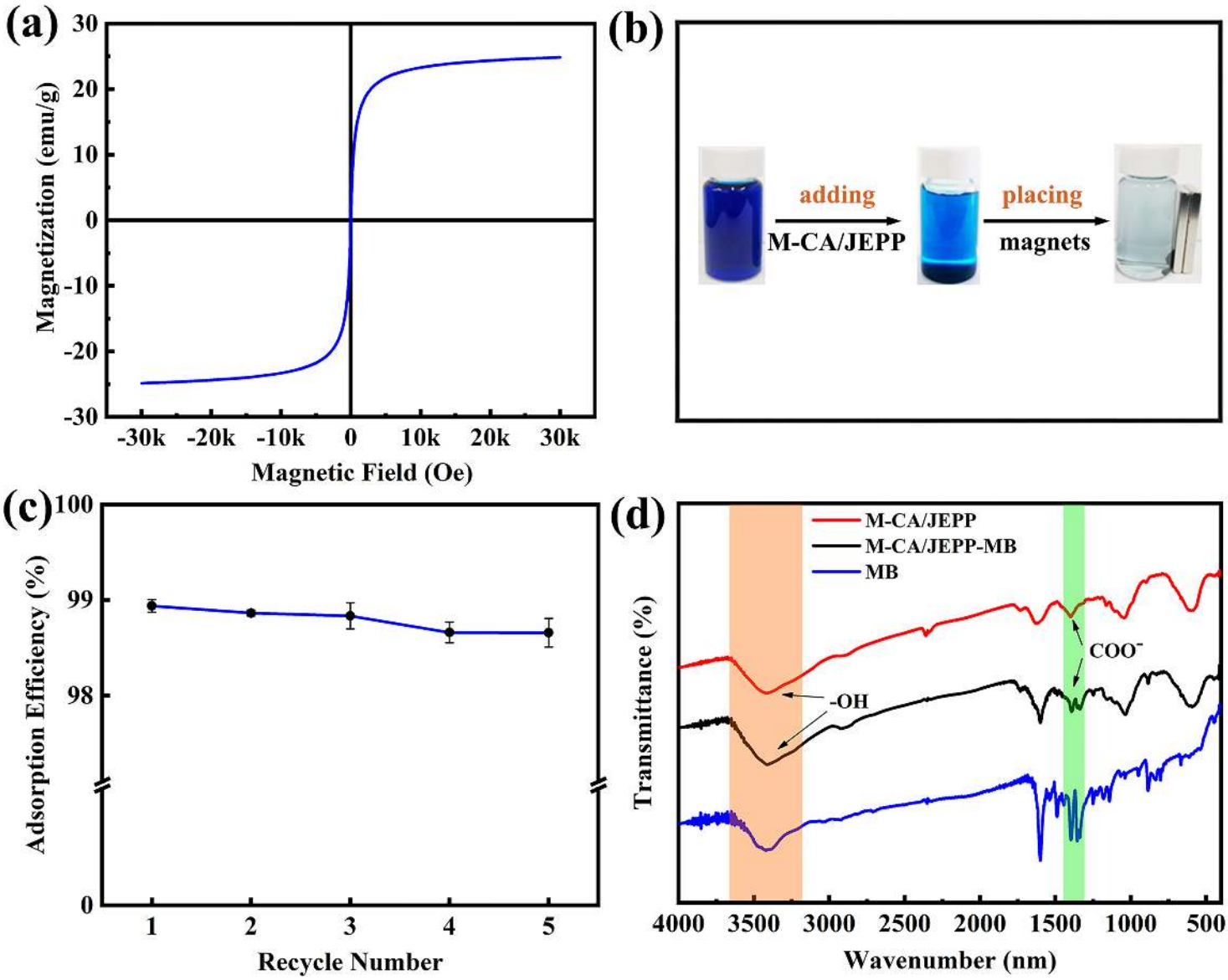


Figure 4

(a) Magnetization curve of M-CA/JEPP. (b) Digital photo of separation after adsorption by magnets, initial pH=11, initial dye concentration of 50 mg/L, 303 K and 10 mg of adsorbents. (c) Regeneration performance of M-CA/JEPP. (d) FTIR spectra of M-CA/JEPP,M-CA/JEPP-MB, and MB

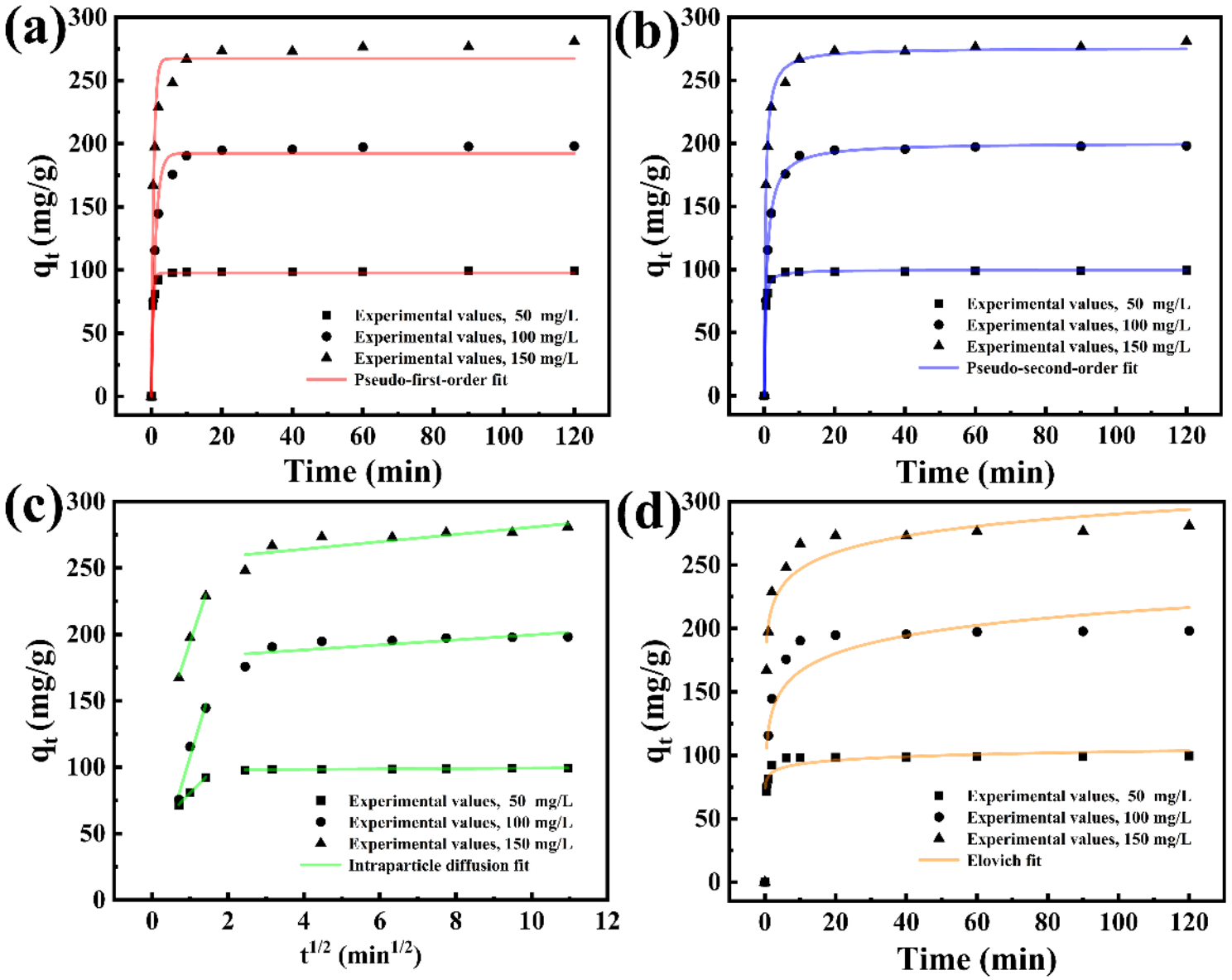


Figure 5

Adsorption kinetics data of M-CA/JEPP for MB fitted with (a) Pseudo-first-order, (b) Pseudo-second-order, (c) Intraparticle diffusion, (d) Elovich

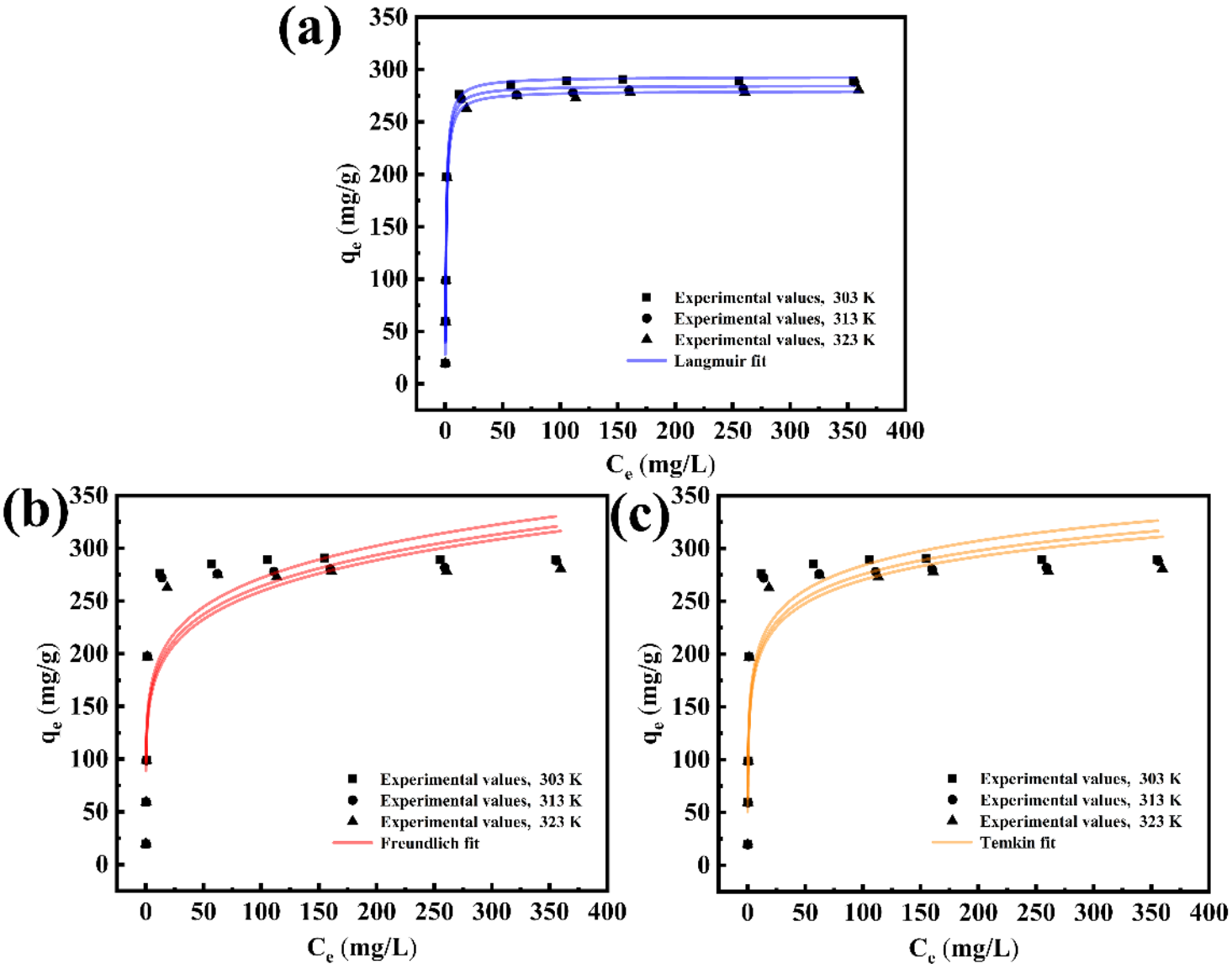


Figure 6

Adsorption isotherm data of M-CA/JEPP for MB fitted with (a) Langmuir, (b) Freundlich, (c) Temkin

Supplementary Files

This is a list of supplementary files associated with this preprint. Click to download.

- SupportingInformation.docx
- Scheme1.png